View metadata, citation and similar papers at core.ac.uk
brought to you by CORE
provided by Elsevier - Publisher Connector

Current Biology 21, 1924–1930, November 22, 2011 ©2011 Elsevier Ltd All rights reserved DOI 10.1016/j.cub.2011.10.012

Report

The Origin of Phragmoplast Asymmetry

Andrei P. Smertenko,[1,2,4] Bernard Piette,[2,3,4] and Patrick J. Hussey[1,2,*]
[1]School of Biological and Biomedical Sciences
[2]Biophysical Sciences Institute
[3]Department of Mathematics
Durham University, Durham DH1 3LE, UK

Summary

The phragmoplast coordinates cytokinesis in plants [1]. It directs vesicles to the midzone, the site where they coalesce to form the new cell plate. Failure in phragmoplast function results in aborted or incomplete cytokinesis leading to embryo lethality, morphological defects, or multinucleate cells [2, 3]. The asymmetry of vesicular traffic is regulated by microtubules [1, 4, 5, 6], and the current model suggests that this asymmetry is established and maintained through treadmilling of parallel microtubules. However, we have analyzed the behavior of microtubules in the phragmoplast using live-cell imaging coupled with mathematical modeling and dynamic simulations and report that microtubules initiate randomly in the phragmoplast and that the majority exhibit dynamic instability with higher turnover rates nearer to the midzone. The directional transport of vesicles is possible because the majority of the microtubules polymerize toward the midzone. Here, we propose the first inclusive model where microtubule dynamics and phragmoplast asymmetry are consistent with the localization and activity of proteins known to regulate microtubule assembly and disassembly.

Results and Discussion

Phragmoplast structure was first studied in fixed cells using electron and immunofluorescence microscopy [1, 5]. Recent studies in living cells have used tubulin and microtubule-associated proteins fused to fluorescent proteins [7, 8]. All approaches indicate that the phragmoplast is a dynamic structure formed at the end of anaphase. A representative sequence in the development of the phragmoplast visualized by fluorescence microscopy in tobacco cells expressing yellow fluorescent protein (YFP)-tubulin is shown in Figure 1A (see also Movie S1 available online). A typical phragmoplast is barrel shaped with the black line across the middle depicting the midzone (frame 8). The midzone represents the site of assembly of vesicles into the growing cell plate, which will eventually separate the daughter cells. Microtubules depolymerize at the sites where cell plate assembly has been completed (Figure 1A, frame 16) making a torus-like structure (Figures 1B and 1C) with new microtubules being formed at the outer edge. Tubulin freed from the depolymerized microtubules is recycled into new microtubules as the phragmoplast grows centrifugally [3]. This results in the outer edge of the torus progressively growing or leading and the inner edge retracting or lagging. The expansion of the phragmoplast stops once the cell plate attaches to the mother cell wall (Figure 1A, frames 28 and 38).

According to the current model [9], the phragmoplast is composed of two interdigitating sets or ringlets of microtubules with the plus end of the ringlets embedded in the developing cell plate material and the microtubules treadmill with new tubulin dimers being added at the plus ends (Figure 1E). This model is consistent with the view that parallel microtubules within each half-set are needed for the directional transport of cell plate components to the midline [4, 5, 6]. However, this model contradicts more recent data where the plus-end tracking protein EB1 is found at the distal edges and throughout the phragmoplast in addition to the midzone labeling [10–13] with EB1 "comets" moving toward the midzone [14]. Similarly, minus-end binding gamma-tubulin ring complex (γ-TuRC) components have been found throughout the phragmoplast (excluding the midzone) in addition to the distal edge [15–20]. Fluorescence recovery after photobleaching (FRAP) analysis of microinjected fluorescently labeled tubulin in *Tradescantia* stamen hair cells is also inconsistent with a microtubule treadmilling model [21]. Taken together, these data indicate that a new model has to be developed to explain phragmoplast dynamics.

We analyzed microtubule dynamics in the phragmoplast using FRAP in tobacco BY-2 cells expressing YFP-tubulin. A rectangular region photobleached in the α-plane (Figure 1C) appears static during the recovery (Figure 2A), and when frames 3, 60, and 169 were colored in green, red, and blue, respectively, and merged, no shift of the photobleached region was apparent (Figure 2B). Moreover, kymographs drawn along four white lines shown in frame 387 demonstrate that the fluorescence signal recovered randomly (Figure 2C). A random recovery of YFP signal was also observed when FRAP was conducted in the γ-plane (Figures 2D and 2E; Movie S2). These findings are not consistent with the treadmilling model in which growing plus ends of microtubules are directed toward the cell plate and depolymerizing minus ends are positioned at the distal edge of the phragmoplast generating a continuous flux of tubulin from the midzone to the distal edge. The lack of tubulin flux suggests that the behavior of individual microtubules is stochastic, that this lack of flux is more consistent with a model where the majority of phragmoplast microtubules undergo dynamic instability, having their minus ends stabilized, and that new microtubules can initiate not only at the midzone, but also at any site within the phragmoplast.

Dynamic instability and treadmilling microtubule behavior in the phragmoplast were compared using FRAP simulations in silico. For a treadmilling model, both the plus and minus ends of microtubules were assumed dynamic; plus ends were set to face the cell plate and persistently grow, whereas the minus ends were set toward the distal edge and depolymerize at the same rate as growth at the plus ends. In this simulation, the bleached region of the phragmoplast translocates away from the midzone (Figures 2F and 2G). The overlay of three differently colored frames demonstrates the shift of the photobleached region during recovery (compare Figure 2H with Figure 2B).

We have examined several sets of parameters where a percentage of the microtubules is set to treadmill and another is set to undergo dynamic instability. The dynamic instability

[4]These authors contributed equally to this work
*Correspondence: p.j.hussey@durham.ac.uk

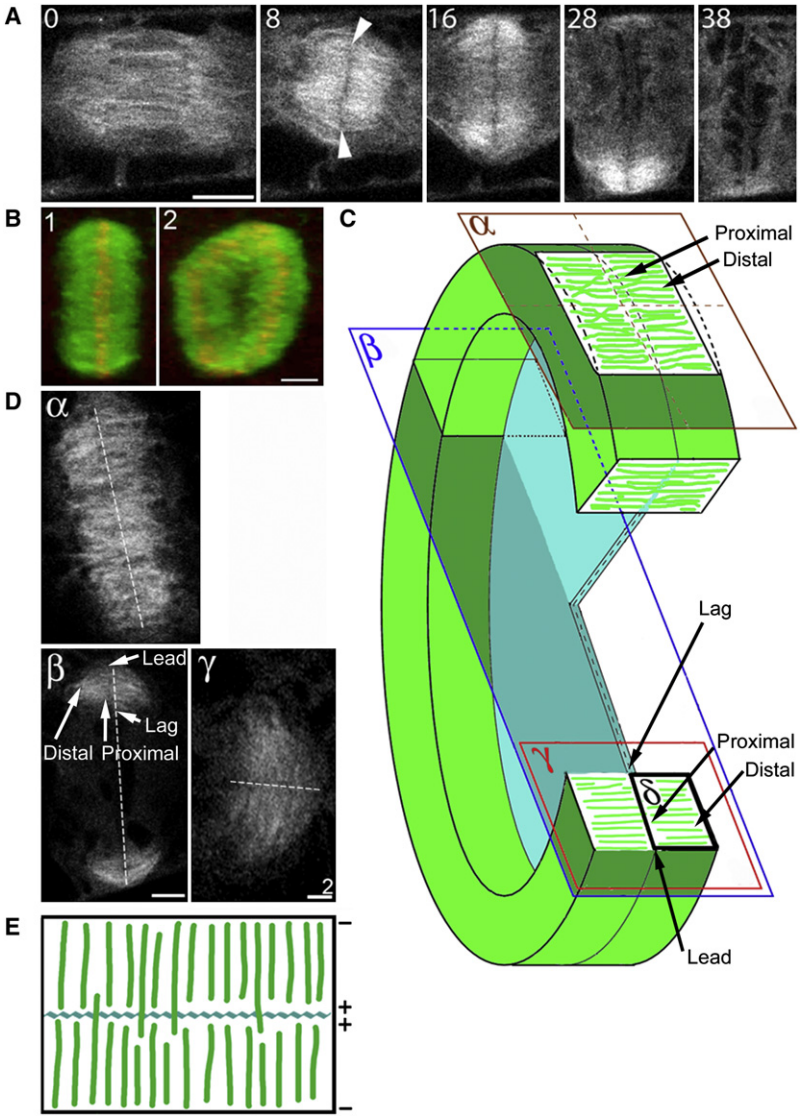

Figure 1. Morphology and Dynamics of the Phragmoplast

(A) Selected frames from an image sequence showing key stages of phragmoplast development in tobacco BY-2 cells expressing YPF-tubulin. Numbers represent time in seconds. Frame 0 shows the anaphase spindle; frame 8 shows the barrel-shaped phragmoplast (arrowheads mark the midzone); frame 16 shows the torus-shaped phragmoplast with reduced density of microtubules in the center; frame 28 shows that cell plate expansion on one side of the phragmoplast has finished and the microtubules depolymerized; frame 38 shows that cell plate formation is complete and all microtubules have depolymerized. Scale bar represents 10 μm.

(B) Three-dimensional reconstruction of the expanding torus-shaped phragmoplast. Microtubules are stained green with anti-tubulin antibody, and the midzone is stained red with an antibody against the microtubule-associated protein MAP65-3 [28, 29]. Scale bar represents 10 μm. Panel 1 shows the top view of the phragmoplast; panel 2 is a 45° rotation of the same image showing loss of microtubules in the center of the phragmoplast.

(C) Diagram of an expanding phragmoplast. Microtubules are shown in green, and the cell plate is shown in cyan. The planes used in the experiments are marked as follows: α, β, γ, and δ.

(D) Images of the phragmoplast in α-, β-, and γ-planes as indicated in (C). Broken line marks the position of the midzone.

(E) Schematic representation of phragmoplast structure. Microtubules (drawn in green) are perpendicular to the midzone, which is shown in cyan. The plus ends of the microtubules are oriented toward the midzone.

model assumes a stochastic transition between the growth and shrinkage phases at the plus ends of individual microtubules, whereas minus ends are capped by the gamma-tubulin ring complex and therefore are not dynamic. All simulations included a 500 s period before photobleaching to allow polymerization reactions to reach the steady state. The simulations were performed with and without the microtubule pausing phase, and the FRAP pattern was found to be identical in both cases. In all simulations where the proportion of treadmilling microtubules is set at 5% and below, the recovery pattern was found to be indistinguishable from our experimental data (compare Figures 2I–2K with Figure 2B; Figure S1). In the simulations where the proportion of treadmilling microtubules exceeded 5% (Figure S1), the translocation of the photobleached region from the treadmilling fraction of microtubules away from the midzone results in an apparent oblique black line similar to the one shown in Figure 2G. This line was not observed in the FRAP experiments, which demonstrates that the fraction of treadmilling microtubules does not exceed 5%.

The simulations suggest that the direction of microtubule polymerization is random in the phragmoplast, and this raises the question of how directional transport will occur along microtubules. It is plausible that some microtubules are initiated and have their plus ends attached to the cell plate for a length of time sufficient for directional transport and that we miss these events in the FRAP experiments as a result of the dynamics and/or density of microtubules. To address this hypothesis, we reduced microtubule dynamics using taxol, and the effect on the recovery of the signal was examined. Taxol is known to inhibit microtubule depolymerization, and it can block cell plate synthesis [3]. Although treatment with 10 μM taxol completely stopped phragmoplast expansion, 5 μM taxol reduced the rate of expansion by 2-fold from 0.66 ± 0.29 μm/min (n = 15) in control to 0.29 ± 0.20 μm/min (n = 12) in taxol-treated cells (Figure S2A). Analysis of time-lapse images confirms that cells are able to proceed from anaphase to telophase (Figure 3A). Following the anaphase spindle, all midzone microtubules gradually depolymerize (starting from frame 9'51" in Figure 3A) and a phragmoplast is formed by microtubules growing from the distal edges toward the midzone (Figure 3A, frames 17'23" and 23'46"; Movie S3). Although the phragmoplast morphology was normal at the early stages (frame 42'55"), at the later stages, the microtubules at the leading edges were more curved. The proportion of YFP-tubulin incorporated into microtubules increased from 82.1% ± 11.4% (n = 18) to 93% ± 4.9% (n = 15), and tubulin turnover ($t_{1/2}$) slowed down from 40.9 ± 17.2 s (n = 18) in the control to 180.5 ± 93.9s (n = 15). The width and thickness of the phragmoplast were not affected by taxol treatment (Figure S2B), demonstrating that phragmoplast dimensions do not depend on the dynamic state of microtubules. Depolymerization of actin filaments

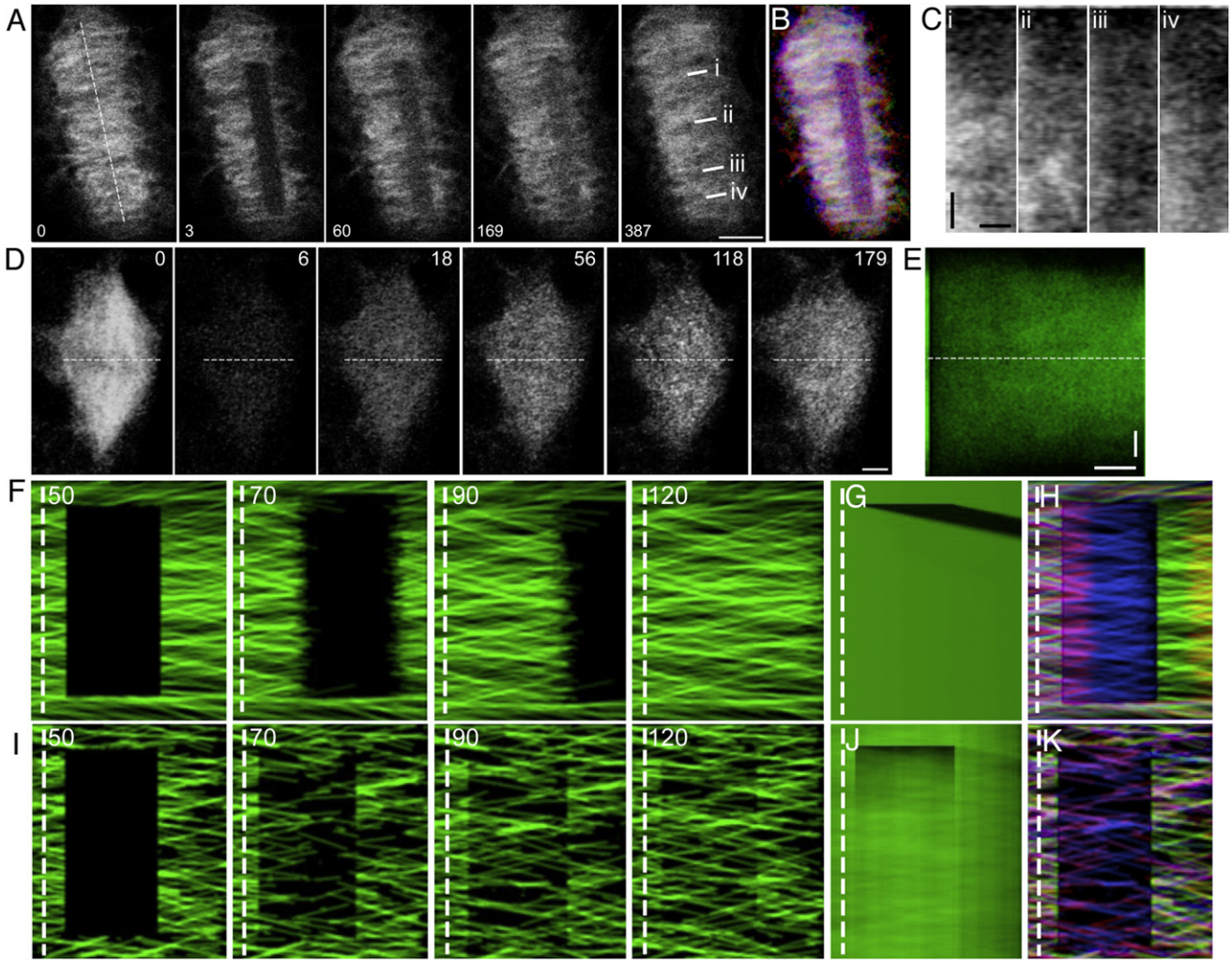

Figure 2. Analysis of Microtubule Polymerization in the Expanding Phragmoplasts

(A) Selected frames from a phragmoplast fluorescence recovery after photobleaching (FRAP) experiment conducted in plane α as shown in Figure 1C. Frame 0 was taken before the photobleach, and frame 3 was taken afterwards. Scale bar represents 5 μm.

(B) Frames 3, 60, and 169 were colored in green, red, and blue, respectively, and merged.

(C) Kymographs recorded along lines i, ii, iii, and iv shown in frame 387. The vertical scale bar corresponds to 60 s, and the horizontal scale bar corresponds to 4 μm. The left edge of each kymograph is proximal to the midzone.

(D) Selected frames from a FRAP experiment performed in plane γ (Figure 1C). Scale bar represents 2 μm.

(E) Average kymograph of the experiment shown in (D). The vertical scale bar is 2 μm, and the horizontal scale bar is 60 s.

(F and K) Simulation of FRAP experiment where all (F–H) or 5% of microtubules (I–K) are treadmilling.

(F and I) Individual frames. The left edge of the kymograph is proximal to the midzone. The simulation corresponds to plane δ.

(G and J) Average kymographs. Translocation of the bleached region toward the distal part of the phragmoplast is apparent only when microtubules are treadmilling (G).

(H and K) Frames 50, 70, and 90 in (F) and (I) were colored in green, red, and blue, respectively, and merged.

Numbers in the individual frames represent relative time in seconds from the start point. The broken lines mark the position of the midzone.

with drugs Cytochalasin D and Latrunculin B cause a reduction in phragmoplast width (Figure S2C), indicating that actin filaments are important for the control of phragmoplast size.

Taxol treatment has a profound effect on the FRAP pattern. Figures 3B and 3C show that recovery in the γ-plane starts at the midzone and expands toward the edges, suggesting that microtubule nucleation occurs preferentially at the midzone (Movie S4). However, the bleached region does not translocate (Figures 3D and 3E), demonstrating that stabilization of microtubules and reduction of microtubule dynamics still does not cause treadmilling. The rates of microtubule turnover in the photobleached whole, proximal, and distal regions were compared in both control and 5 μM taxol-treated samples (Figure 4A). The turnover rate in the distal region of the control samples was 12% slower than the proximal region (n = 18), and taxol amplified this difference to 52% (n = 13; Figure 4B). Therefore, the faster signal recovery near the midzone of the phragmoplast in taxol-treated cells is due to a faster turnover of microtubules.

These differences in microtubule turnover between the distal and proximal regions highlight the asymmetry in phragmoplast organization. Several factors can cause this asymmetry: first, the distribution and activity of γ-TuRC, which is responsible for the nucleation of microtubules. Gamma tubulin

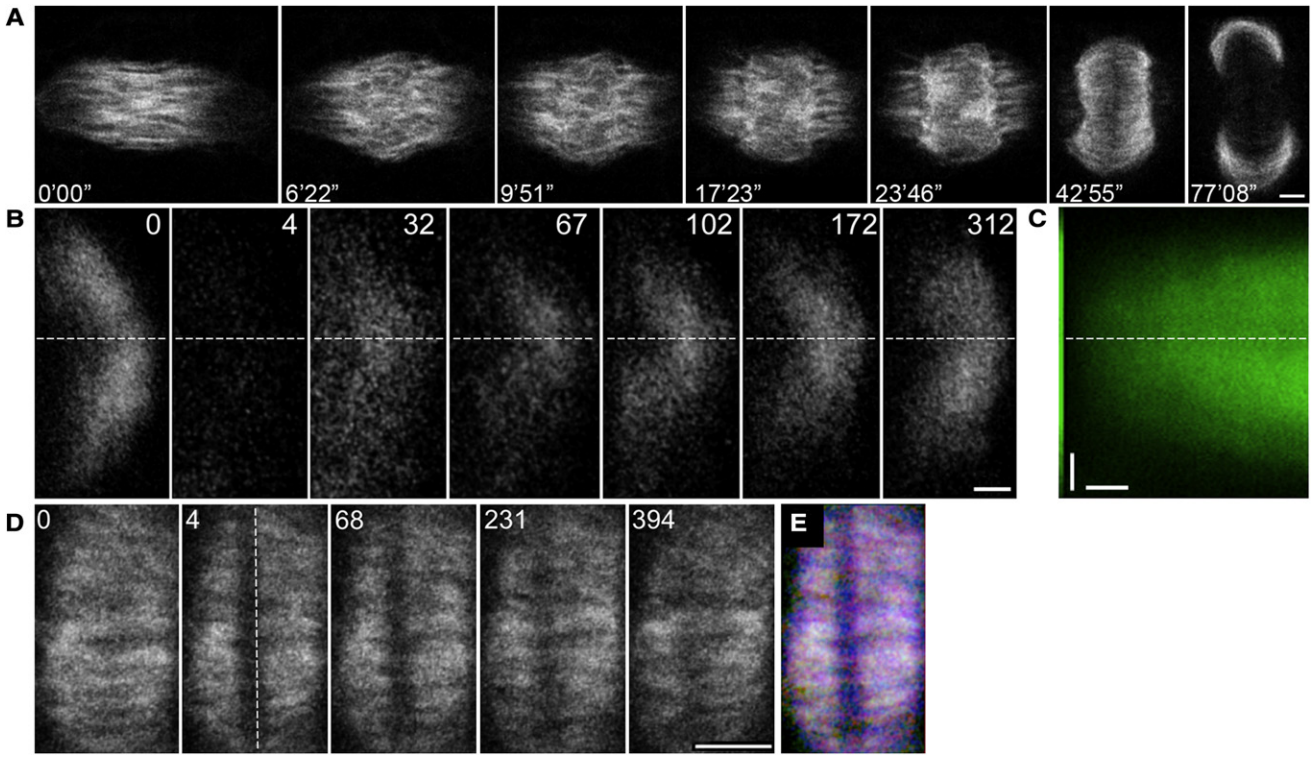

Figure 3. Effect of 5 μM Taxol on the Tubulin Turnover in the Phragmoplast

(A) Selected frames from a movie showing the transition of a cell from anaphase to telophase in plane β. Scale bar represents 5 μm. Numbers in each frame show relative time in minutes and seconds.

(B) Selected frames from a FRAP experiment performed in plane γ (Figure 1C). Scale bar represents 2 μm. Frames 0 and 4 are taken before and after the photobleach.

(C) Average kymograph of the experiment shown in (B). Vertical scale bar represents 2 μm, and horizontal scale bar represents 60 s.

(D) Selected frames from a FRAP experiment performed in plane α. Scale bar represents 10 μm.

(E) Frames 4, 68, and 231 were colored in green, red, and blue, respectively, and merged.

Numbers in the individual frames represent relative time in seconds from the start point. The broken lines mark the position of the midzone.

and other members of γ-TuRC localize near the cell plate and the distal edge of the phragmoplast but are also observed along the length of phragmoplast microtubules [15–20], suggesting that microtubules can be nucleated randomly or be biased toward a particular site. Second, microtubule minus ends can be capped by γ-TuRC and remain stable, allowing dynamics only at the plus ends or can be free leading to treadmilling, which has been reported for interphase microtubules [20, 22]. Third, the direction of polymerization and consequently the orientation of microtubules could be preferentially towards or away from the midzone. End binding proteins that preferentially associate with the growing ends of microtubules can mark the direction of their polymerization (reviewed in [23]). Immunolabeling and live-cell imaging unequivocally demonstrate the presence of end binding proteins at the proximal region, distal edge, and along phragmoplast microtubules [10–13], which suggests that microtubules can polymerize in either direction and have mixed polarity. However, vesicle trafficking must occur with a net flow toward the midzone in order for cell plate synthesis to occur. Fourthly, stability of the microtubules can be dependent on the distance from the midzone. In yeast mitotic spindles, for example, microtubule ends proximal to the midzone are more likely to undergo catastrophe and therefore are more dynamic in comparison to the ends in the distal region [24, 25].

In order to assess which of these factors contribute to the establishment and maintenance of phragmoplast asymmetry, we have modeled each individually or in a variety of combinations. A detailed description of 17 different scenarios is provided in Supplemental Results, Data Set 1, but put briefly, we have explored the following hypotheses: (1) microtubules are seeded differentially in the distal and proximal regions (simulations sB, sC, sD, sE, sF); (2) microtubules are seeded randomly but preferentially polymerize in one direction either toward the midzone or distal zone (sA); (3) there is a difference in the catastrophe rates of microtubules in the proximal and/or distal regions (sG, sH, sI); (4) a combination of the above as follows: microtubules are more stable near the midzone and the majority polymerize in one direction in sJ, microtubules are more stable near the midzone and a fraction is nucleated at the distal edge in sK, microtubules are more stable near the midzone and a fraction is nucleated near the midzone in sL, the nucleation of microtubules is dependent on the distance from the midzone and the majority polymerise in one direction in sM, and a fraction of microtubules is nucleated at the distal edge and the rest are nucleated dependent on the distance from the midzone in sN; and (5) all plus ends of microtubules are dynamic and face the cell plate, some minus ends are either capped by γ-TuRC and are nondynamic, whereas some minus ends are free and undergo dynamic instability (sO, sP, and sQ). In the latter scenario, the three simulations

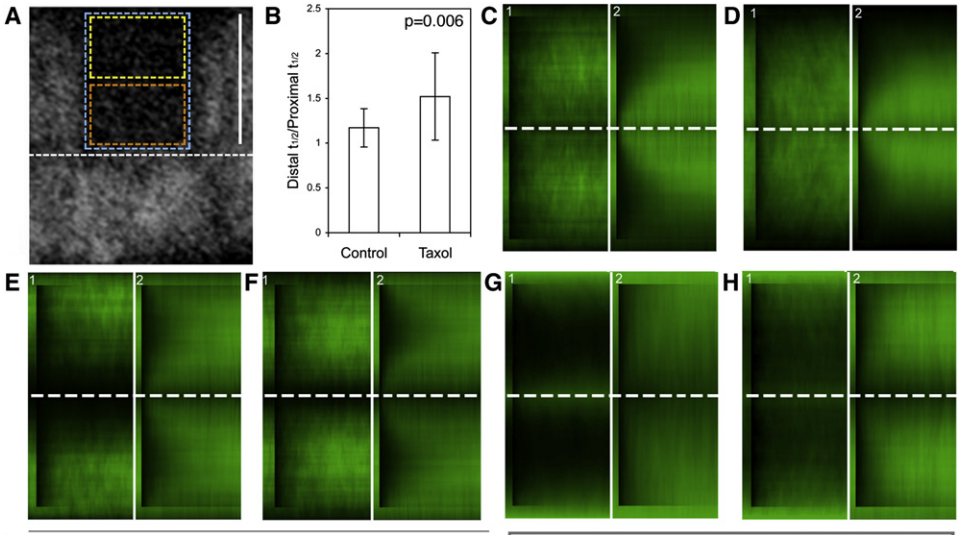

I

Event	Plus end	Minus end
Growth	k_+ = 0.0600 µm/s	k_+= 0.0327 µm/s
Growth/shortening	K_{gs}= 0.0250/s	K_{gs}= 0.1000/s
Growth/pause	K_{gp}= 0.1200/s	K_{gp}= 0.0560/s
Pause/growth	K_{pg}= 0.0840/s	K_{pg}= 0.0065/s
Pause/shortening	K_{ps}= 0.0400/s	K_{ps}= 0.0330/s
Shortening/pause	K_{sp}= 0.0156/s	K_{sp}= 0.0720/s
Shortening/growth	K_{sg}= 0.0590/s	K_{sg}= 0.0390/s
Shortening	k.= 0.1000 µm/s	k.= 0.0460 µm/s

J

Event	Plus end	Minus end
Growth	k_+ = 0.0600 µm/s	k_+= 0.0327 µm/s
Growth/shortening	K_{gs}= 0.0161/s	K_{gs}= 0.0654/s
Growth/pause	K_{gp}= 0.0774/s	K_{gp}= 0.0361/s
Pause/growth	K_{pg}= 0.1302/s	K_{pg}= 0.0101/s
Pause/shortening	K_{ps}= 0.0258/s	K_{ps}= 0.0213/s
Shortening/pause	K_{sp}= 0.0242/s	K_{sp}= 0.1116/s
Shortening/growth	K_{sg}= 0.0915/s	K_{sg}= 0.0605/s
Shortening	k.= 0.1000 µm/s	k.= 0.0460 µm/s

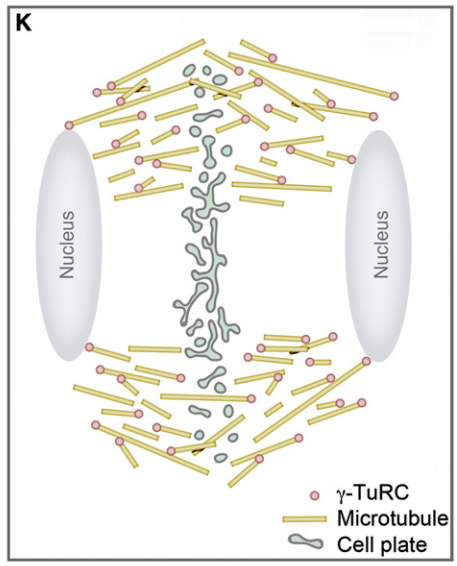

Figure 4. Comparison of Tubulin Turnover in the Phragmoplast Proximal and Distal Regions

(A) A time frame from the FRAP experiment. The recovery of fluorescent signal was measured in the proximal region (orange rectangle) and distal (yellow rectangle) region. The whole photobleached region is marked by a blue rectangle, and the white line shows the position of the midzone.

(B) The ratio of the fluorescence signal turnover time ($t_{1/2}$) in the proximal and distal parts of the phragmoplast in control and 5 µM taxol-treated cells. Error bars show the standard deviation of the mean.

(C–H) Average kymographs of simulated FRAP experiments in control (panel 1) and taxol-treated (panel 2) samples where 67% of microtubules grow toward and 33% grow away from the midzone (C; simulations sA in Figure S4), 70% of microtubules grow on both ends and the rest are attached to the gamma-tubulin ring complex (γ-TuRC) and can only grow on the plus end (D; simulation sQ), the nucleation rate of microtubules increases toward the distal zone (E; simulation sD), microtubules are stabilized in the proximal zone (F; simulation sH), 70% of microtubules are seeded at the distal edge of phragmoplast and the rest are seeded at the cell plate (G; simulation sC), 12.5% of microtubules are seeded at the cell plate, 37.5% of microtubules are seeded at the distal edge, and the rest are seeded randomly in between (H; simulation sF).

(I and J) Parameters of microtubule dynamics used in the simulation sQ (D) of control (I) and taxol treatment (J) condition.

(K) Model of microtubule organization in the phragmoplast. Microtubules are nucleated on γ-TuRC located either on the extant microtubules (with the same polarity as the mother microtubule) or free, generating microtubules of random polarity. Severing of microtubules can produce fragments with both ends dynamic.

have slightly different parameters where the stability of microtubule ends is dependent on contact with membrane (cell plate or nucleus). Within each simulation, several parameters were adjusted to match the experimentally defined turnover rates of microtubules and the difference between the rates in the proximal and distal regions in control and taxol-treated cells.

We have optimized parameter sets in sixteen distinct scenarios to match the quantitative YFP-tubulin turnover rates in the proximal and distal regions; however, the kymographs of only four sets show qualitative parity with the experimental kymographs (Figures 4C and 4D; Figure S4, first row, simulations sA, sM, sO, and sQ). In all four sets, microtubules are seeded randomly and polymerize both toward and away

from the midzone; however, more microtubules polymerize toward the cell plate and with higher rates. This occurs either when only the plus ends grow and 67% of microtubules polymerize toward the cell plate (simulations sA and sM) or when both ends of the microtubules grow (simulations sO and sQ). In the latter case, the phragmoplast asymmetry results from the fact that the dynamics at the plus ends are greater than at the minus ends. In these simulations, microtubules have various lengths, but the average value is shorter than the width of the phragmoplast (Figure S3). In the other sets, either no difference was observed between the control and taxol-treated cell kymographs or both kymographs did not resemble the experimental data (Figures 4E–4H; Figure S4). Modulation of the parameters of microtubule dynamics alone can significantly affect phragmoplast morphology by increasing the width of the midzone (Figures 4E and 4F) or concentrating microtubules in the midzone (Figures 4G and 4H). Therefore, the asymmetry in phragmoplast architecture is generated not via the uneven nucleation of microtubules or their differential stabilization but by a higher amount of microtubule polymerization toward the cell plate than toward the nuclei.

Plant microtubules are nucleated by the gamma-tubulin complexes on the nuclear surface [26], on the surface of existing microtubules [10, 20], and at random locations in the cytoplasm [10, 22]. Following nucleation, microtubules can be severed, generating fragments with dynamic minus ends [20, 22]. In the interphase cortical array, extant microtubules serve as a major template for the nucleation of new microtubules [10], and in this case, the polarity of daughter microtubules resembles the polarity of the mother microtubule. In this way, the overall polarity of microtubules in an array can persist even when all the original microtubules depolymerize. Conceivably, the orientation of microtubule minus ends is biased toward the forming nuclei during anaphase B where microtubules are nucleated by kinetochores and spindle poles. This asymmetry of microtubule polarity is templated through cytokinesis. Consistently, the majority of microtubule plus ends in the phragmoplasts of sunflower endosperm cells face the cell plate, but a significant proportion of microtubules have opposite polarity and polymerize away from the midzone [6]. Severing generates free minus ends, which can elongate toward the distal edge of the phragmoplast. Microtubule severing is important for cytokinesis because deletion of katanin leads to abnormal phragmoplast morphology [27]. Therefore, microtubules of mixed polarity polymerizing at the plus ends and capped by γ-TuRC at the minus end, as suggested by simulations sA and sM, and microtubules with dynamic plus and minus ends, as in simulations sO and sQ, are likely to play a role in phragmoplast organization and dynamics.

We propose a new model for phragmoplast organization based on dynamic instability (Figure 4K). In this model, microtubules do not have a preferential nucleation site in the phragmoplast but can be nucleated anywhere along the extant microtubules, the surface of the forming nuclei, and the free gamma-tubulin ring complexes. The polarity of phragmoplast microtubules is established during anaphase B when microtubule minus ends bias toward the segregated chromosomes. Nucleation along the extant microtubules and nuclear surface generates microtubules of the same polarity and maintains the asymmetry of microtubule organization during cytokinesis, whereas "free" nucleation produces microtubules of random polarity. Severed microtubules can polymerize on both ends and in some instances undergo treadmilling. The bulk of microtubule polymerization occurs toward the midzone. This creates and maintains the asymmetry of microtubule organization in the phragmoplast and allows plus-end-directed kinesins to orchestrate vesicle traffic toward the midzone for cell plate assembly and at the same time allows for some vesicle traffic to occur away from the midzone by similar motors. The average length of the microtubules is less than the phragmoplast thickness, and phragmoplast dimensions are determined by the balance of the pushing force of polymerizing microtubules and the pressure exerted by the vacuole and nuclei.

Supplemental Information

Supplemental Information includes four figures, Supplemental Results, Supplemental Experimental Procedures, and four movies and can be found with this article online at doi:10.1016/j.cub.2011.10.012.

Acknowledgments

We are grateful to Takashi Hashimoto for the YFP-tubulin BY-2 cell line. B.P. was supported by the Science and Technology Facilities Council grant ST/H003649/1.

Received: July 11, 2011
Revised: September 9, 2011
Accepted: October 6, 2011
Published online: November 10, 2011

References

1. Gunning, B.E.S. (1982). The cytokinetic apparatus: its development and spatial regulation. In The Cytoskeleton in Plant Growth and Development, C.W. Lloyd, ed. (London: Academic press), pp. 229–292.
2. Jürgens, G. (2005). Cytokinesis in higher plants. Annu. Rev. Plant Biol. *56*, 281–299.
3. Yasuhara, H., Sonobe, S., and Shibaoka, H. (1993). Effects of taxol on the development of the cell plate and of the phragmoplast in tobacco BY-2 cells. Plant Cell *34*, 21–29.
4. Lloyd, C., and Hussey, P. (2001). Microtubule-associated proteins in plants—why we need a MAP. Nat. Rev. Mol. Cell Biol. *2*, 40–47.
5. Samuels, A.L., Giddings, T.H., Jr., and Staehelin, L.A. (1995). Cytokinesis in tobacco BY-2 and root tip cells: a new model of cell plate formation in higher plants. J. Cell Biol. *130*, 1345–1357.
6. Euteneuer, U., Jackson, W.T., and McIntosh, J.R. (1982). Polarity of spindle microtubules in *Haemanthus* endosperm. J. Cell Biol. *94*, 644–653.
7. Granger, C.L., and Cyr, R.J. (2000). Microtubule reorganization in tobacco BY-2 cells stably expressing GFP-MBD. Planta *210*, 502–509.
8. Ueda, K., Sakaguchi, S., Kumagai, F., Hasezawa, S., Quader, H., and Kristen, U. (2003). Development and disintegration of phragmoplasts in living cultured cells of a GFP:TUA6 transgenic Arabidopsis thaliana plant. Protoplasma *220*, 111–118.
9. Asada, T., Sonobe, S., and Shibaoka, H. (1991). Microtubule translocation in the cytokinetic apparatus of cultured tobacco cells. Nature *350*, 238–241.
10. Chan, J., Calder, G.M., Doonan, J.H., and Lloyd, C.W. (2003). EB1 reveals mobile microtubule nucleation sites in Arabidopsis. Nat. Cell Biol. *5*, 967–971.
11. Van Damme, D., Bouget, F.-Y., Van Poucke, K., Inzé, D., and Geelen, D. (2004). Molecular dissection of plant cytokinesis and phragmoplast structure: a survey of GFP-tagged proteins. Plant J. *40*, 386–398.
12. Chan, J., Calder, G., Fox, S., and Lloyd, C. (2005). Localization of the microtubule end binding protein EB1 reveals alternative pathways of spindle development in Arabidopsis suspension cells. Plant Cell *17*, 1737–1748.
13. Bisgrove, S.R., Lee, Y.-R.J., Liu, B., Peters, N.T., and Kropf, D.L. (2008). The microtubule plus-end binding protein EB1 functions in root responses to touch and gravity signals in Arabidopsis. Plant Cell *20*, 396–410.
14. Ho, C.M., Hotta, T., Guo, F., Roberson, R.W., Lee, Y.R., and Liu, B. (2011). Interaction of antiparallel microtubules in the phragmoplast is mediated by the microtubule-associated protein MAP65-3 in Arabidopsis. Plant Cell *23*, 2909–2923.

15. Liu, B., Joshi, H.C., Wilson, T.J., Silflow, C.D., Palevitz, B.A., and Snustad, D.P. (1994). γ-Tubulin in Arabidopsis: gene sequence, immunoblot, and immunofluorescence studies. Plant Cell *6*, 303–314.
16. Dryková, D., Cenklová, V., Sulimenko, V., Volc, J., Dráber, P., and Binarová, P. (2003). Plant γ-tubulin interacts with alphabeta-tubulin dimers and forms membrane-associated complexes. Plant Cell *15*, 465–480.
17. Kumagai, F., Nagata, T., Yahara, N., Moriyama, Y., Horio, T., Naoi, K., Hashimoto, T., Murata, T., and Hasezawa, S. (2003). Gamma-tubulin distribution during cortical microtubule reorganization at the M/G1 interface in tobacco BY-2 cells. Eur. J. Cell Biol. *82*, 43–51.
18. Zeng, C.J.T., Lee, Y.-R.J., and Liu, B. (2009). The WD40 repeat protein NEDD1 functions in microtubule organization during cell division in Arabidopsis thaliana. Plant Cell *21*, 1129–1140.
19. Kong, Z., Hotta, T., Lee, Y.-R.J., Horio, T., and Liu, B. (2010). The γ-tubulin complex protein GCP4 is required for organizing functional microtubule arrays in Arabidopsis thaliana. Plant Cell *22*, 191–204.
20. Nakamura, M., Ehrhardt, D.W., and Hashimoto, T. (2010). Microtubule and katanin-dependent dynamics of microtubule nucleation complexes in the acentrosomal Arabidopsis cortical array. Nat. Cell Biol. *12*, 1064–1070.
21. Hush, J.M., Wadsworth, P., Callaham, D.A., and Hepler, P.K. (1994). Quantification of microtubule dynamics in living plant cells using fluorescence redistribution after photobleaching. J. Cell Sci. *107*, 775–784.
22. Shaw, S.L., Kamyar, R., and Ehrhardt, D.W. (2003). Sustained microtubule treadmilling in Arabidopsis cortical arrays. Science *300*, 1715–1718.
23. Akhmanova, A., and Steinmetz, M.O. (2008). Tracking the ends: a dynamic protein network controls the fate of microtubule tips. Nat. Rev. Mol. Cell Biol. *9*, 309–322.
24. Maddox, P.S., Bloom, K.S., and Salmon, E.D. (2000). The polarity and dynamics of microtubule assembly in the budding yeast Saccharomyces cerevisiae. Nat. Cell Biol. *2*, 36–41.
25. Pearson, C.G., Gardner, M.K., Paliulis, L.V., Salmon, E.D., Odde, D.J., and Bloom, K. (2006). Measuring nanometer scale gradients in spindle microtubule dynamics using model convolution microscopy. Mol. Biol. Cell *17*, 4069–4079.
26. Seltzer, V., Janski, N., Canaday, J., Herzog, E., Erhardt, M., Evrard, J.-L., and Schmit, A.-C. (2007). Arabidopsis GCP2 and GCP3 are part of a soluble γ-tubulin complex and have nuclear envelope targeting domains. Plant J. *52*, 322–331.
27. Panteris, E., Adamakis, I.-D.S., Voulgari, G., and Papadopoulou, G. (2011). A role for katanin in plant cell division: microtubule organization in dividing root cells of fra2 and lue1Arabidopsis thaliana mutants. Cytoskeleton (Hoboken) *68*, 401–413.
28. Müller, S., Smertenko, A., Wagner, V., Heinrich, M., Hussey, P.J., and Hauser, M.-T. (2004). The plant microtubule-associated protein AtMAP65-3/PLE is essential for cytokinetic phragmoplast function. Curr. Biol. *14*, 412–417.
29. Smertenko, A.P., Kaloriti, D., Chang, H.-Y., Fiserova, J., Opatrny, Z., and Hussey, P.J. (2008). The C-terminal variable region specifies the dynamic properties of Arabidopsis microtubule-associated protein MAP65 isotypes. Plant Cell *20*, 3346–3358.